International Journal of Biological Macromolecules 282 (2024) 137305

Contents lists available at ScienceDirect

International Journal of Biological Macromolecules

journal homepage: www.elsevier.com/locate/ijbiomac

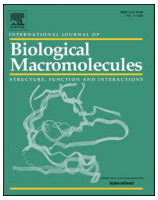

Pharmacokinetics and fate of free and encapsulated IRD800CW-labelled human BChE intravenously administered in mice

Tatiana Pashirova [a,b,*], Zukhra Shaihutdinova [a,b], Dmitry Tatarinov [b], Angelina Titova [a], Albina Malanyeva [a], Olga Vasileva [a], Kamil Gabdurakhmanov [a], Sergei Dudnikov [a], Lawrence M. Schopfer [c], Oksana Lockridge [c], Patrick Masson [a,**]

[a] Institute of Fundamental Medicine and Biology, Kazan Federal University, 420008 Kazan, 18 Kremlyovskaya St., Russian Federation
[b] Arbuzov Institute of Organic and Physical Chemistry, FRC Kazan Scientific Center of RAS, Arbuzov Str. 8, 420088 Kazan, Russian Federation
[c] University of Nebraska Medical Center, Eppley Institute, Omaha, NE, USA

ARTICLE INFO

Keywords:
Butyrylcholinesterase
Bioscavenger
Infrared probe
Pharmacokinetics
Polymersomes

ABSTRACT

Human butyrylcholinesterase (BChE) is an efficient bioscavenger of toxicants. Highly purified BChE was labelled with the near infrared fluorescent IRDye800CW. The goal was to determine the pharmacokinetics and fate of enzyme in mice. BChE-IRDye800CW was encapsulated in polyethylene glycol−polypropylene sulfide-based spherical polymersome nanoreactors with the following characteristics: 140 nm diameter, $\xi = -6$ mV, PDI $\leq$ 0.2, 1 year stability. Encapsulation did not alter the functional properties of BChE. Free and encapsulated enzyme were injected intravenously to CD-1 mice (single dose of enzyme 1.5 mg/kg and PEG-PPS polymersomes 25 mg/kg) and were analyzed for 8 days using an *in vivo* imaging system. Results showed that the pharmacokinetic distribution α-phase of encapsulated BChE ($t_{1/2} = 17.6$ h) was longer than for free enzyme ($t_{1/2} = 6.6$ h). The mean half-time for elimination β-phase was 2-time longer for encapsulated enzyme than for free enzyme (150 *vs* 72 h). Transient changes in infrared fluorescence in organs showed that BChE is eliminated from liver. However, free and encapsulated enzymes were cleared *via* different pathways. This first study of pharmacokinetics and fate of BChE encapsulated in polymersomes initiates research of new formulations of bioscavengers aimed at increasing the residence time of enzymes in the blood stream.

1. Introduction

The highly glycosylated human butyrylcholinesterase (BChE, EC 3.1.1.8; P06276) tetramer of 340 kDa is composed of 4 identical subunits linked through a polyproline peptide [1,2]. BChE is an α/β hydrolase [3] related to acetylcholinesterase (AChE, EC. 3.1.1.7, P22303), the key enzyme of the cholinergic system that terminates the action of the neurotransmitter acetylcholine. Although physiological functions of BChE are still imperfectly known [4], BChE plays a role in the metabolism of numerous drugs and scavenges poisonous esters [5,6]. In particular, its active center serine (S198) is irreversibly phosphylated by organophosphorous compounds (OPs), and thus, BChE acts as an endogenous bioscavenger in first-line defense against these poisonous compounds. In the past 30 years, numerous works have administered highly purified human BChE as an exogenous stoichiometric bioscavenger for prophylaxis and/or post-exposure treatment of OP-poisoning [7–9]. BChE has been converted to a catalytic bioscavenger by mutating Gly117 to His [10] or to a pseudo-catalytic bioscavenger by associating BChE with reactivators [11]. Strategies aimed at increasing the residence time of injected natural or recombinant human BChE include surface chemical modifications (PEGylation [12], polysialylation [13], fusion to other proteins such as albumin [14]),

Abbreviations: BChE, Butyrylcholinesterase; BTC, butyrylthiocholine; CBChE, concentration of BChE; DLS, Dynamic light scattering; EE, encapsulation efficiency %; E-nR, enzyme nanoreactor; IRD800CW, near-infrared dye 800CW; LC, loading capacity; MRT, mean residence time; NIR, near infrared fluorescent probe; nR, nanoreactor; OP, organophosphate; PAS, peripheral anionic site; PBS, phosphate buffer saline; PK, pharmacokinetics; RBC, red blood cell; PPS, polypropylene sulfide; TEM, transmission electron microscopy.

* Corresponding author at: Arbuzov Institute of Organic and Physical Chemistry, FRC Kazan Scientific Center of RAS, Arbuzovstr. 8, Kazan 420088, Russian Federation.
** Corresponding author.
E-mail addresses: tatyana_pashirova@mail.ru (T. Pashirova), pym.masson@free.fr, pmasson@kpfu.ru (P. Masson).

https://doi.org/10.1016/j.ijbiomac.2024.137305
Received 6 August 2024; Received in revised form 3 November 2024; Accepted 4 November 2024
Available online 7 November 2024

encapsulation into regular and bioadhesive liposomes [15,16], polymeric nanoparticles containing a core of protein–polyion complex [17,18], and synthetic membrane-engineering to encapsulate enzymes into RBC [19]. Gene therapy approaches for *in vivo* production of BChE [20] have been undertaken.

Encapsulation of bioscavengers has proven to lead to stable, safe and effective bioscavenger formulations for *in vivo* detoxification of OPs [21] and other toxicants, in particular endogenous reactive oxygen species (ROS) [22], uric acid and other metabolite products [23]. Against exogenous toxicants, the use of injectable enzyme nanoreactors allows fast metabolism of alcohol in cases of extreme alcoholization [24]. Thus, the concept of therapeutic enzyme nanoreactor (*E*-nR) progressively emerged from the concept of enzyme bioscavengers [25]. Then, phosphotriesterase nanoreactors have proven to be effective against acute toxicity of the OP, paraoxon, as prophylaxis and post-exposure treatment [26,27]. To expand the activity spectrum of enzyme nanoreactors against OPs, a mixture of several OP-reacting enzymes can be encapsulated. The present work deals with encapsulation of human BChE in polymersomes, this *E*-nR intended to be used as a fast OP-reacting stoichiometric bioscavenger [7]. Although BChE tetramer displays a high thermodynamic stability [28], its encapsulation in nanoreactors was also expected to increase *in vivo* stability. Moreover, encapsulation of concentrated highly reactive enzymes against OPs (high bimolecular rate constant), working under second-order conditions [25], make enzyme-nanoreactors appealing for fast neutralization of OP molecules *in vivo* [26,27].

Applications of polymersomes as nanoreactors are promising and exciting for the future of nanobiomedicine [30,31]. These nanosystems show multifold advantages over lipid-based nano-structures [32]: nR are more stable compared to liposomes, while membranes of polymersomes are permeable to reactants and enzyme activity is not lost after encapsulation. However, there are still limitations for polymersome-based protein nanocarriers: degradability and production for industrial scale [33]. PEGylated polymersomes are promising for protection against toxicants as they provide long-term action, *i.e.* long circulation time and high enzyme concentration in the bloodstream. Intravenous administration of polyethylene glycol−polypropylene sulfide (PEG-PPS)-based polymersomes at doses of 200 and 20 mg/(kg·week) are well tolerated in mice and in non-human primates. [34]. Although numerous works have been published about the pharmacokinetics (PK) of BChE in rodents, it was important to compare PK profiles, distribution in different organs and fate of injected encapsulated enzyme into PEG-PPS-based polymersomes with injected natural free enzyme. For this purpose, the enzyme was first covalently labelled with the near-infrared fluorescent probe (NIR), IRDye800CW, in a way similar to what was done for horse BChE [17,35,36]. Very recent papers show that the highly sensitive and specific NIR approach has proven to be one of the most powerful tools for studying the fate of injected exogenous BChE, for imaging distribution and level of the enzyme under pathological states and for screening of ligands of pharmacological interest [37,38]. Here NIR-labelled BChE allowed access to real-time distribution of injected enzyme in the body and residence times in blood and organs. The PK in mouse blood of injected free human BChE compared to injected BChE-loaded polymersomes, distribution of fluorescence in organs and elimination of the enzyme were analyzed up to 8 days. To summarize, the present work shows that encapsulated BChE in polymersome nanoreactors is functional and display no alteration in its catalytic behavior. Pharmacokinetic study and organ distribution of BChE indicate that the encapsulated enzyme has a longer residence time in blood than the free enzyme, and is eliminated from liver is a monophasic pathway different from the free enzyme.

2. Materials and methods

2.1. Chemicals

Butyrylthiocholine iodide (BTC) and dithio-bis-nitrobenzoic acid (DTNB) were from Sigma-Aldrich, Saint-Louis, MO, USA. Stock solutions of BTC (0.1 M) prepared in water was stored at −20 °C. Poly(ethylene glycol) methyl ether ($mPEG_{750}$, average Mn = 750 from here and below $mPEG_{17}$-OH and $mPEG_{2000}$; average Mn = 2000 from here and below $mPEG_{45}$-OH, Sigma-Aldrich, USA), Propylene Sulfide (stabilized with Butyl Mercaptan) (PS, Tokyo Chemical Industry Co., Ltd., Tokyo, Japan), Potassium thioacetate (98 %, Sigma-Aldrich, Switzerland). All other chemicals and solvents were of chemical or biochemical grade. Ultra-purified water (18.2 MΩ cm resistivity at 25 °C) was produced from Direct-Q 5 UV equipment (Millipore S.A.S. 67120 Molsheim, France). IRDye800CW NHS Ester (LI-COR Biosciences, Lincoln, NE, USA).

2.2. Butyrylcholinesterase preparation

Human BChE tetramer (340 kDa) from plasma of blood donors was highly purified to homogeneity by affinity chromatography on Hupresin gel. The starting material was pooled Cohn fraction IV-4 [39]. The specific activity of the preparation with 1 mM BTC was 3386 units/mL PBS with 1 mM BTC as the substrate [40] at 25 °C (one unit corresponds to the number of micromoles of BTC hydrolyzed per minute), 6.8 mg/mL, *i.e.* 0.5 units/μg. The enzyme was free of detectable contaminants on polyacrylamide gels stained for proteins with Coomassie Brilliant Blue (SDS gel) and for activity with 1 mM BTC as the substrate (native gel) (SM, Figs. S1, S2).

2.3. BChE activity measurements

Standard BChE activity was measured by the Ellman method [40] with 1 mM BTC as the substrate in 0.1 M phosphate buffer pH 7.0 at 25 °C. A thermostated double beam spectrophotometer at λ = 412 nm was used.

For steady-state kinetic analysis of free and encapsulated enzyme, kinetics were measured over a wide range of BTC concentrations (5 to 10,000 μM). Catalytic parameters were determined using the Radic equation (Eq. (1)) that conveniently describes the catalytic behavior of BChE with charged substrates like BTC [5].

$$v = \left(\frac{k_{cat}[E]}{1 + K_m/[S]}\right)\left(\frac{1 + b[S]/K_{ss}}{1 + [S]/K_{ss}}\right) \quad (1)$$

where k_{cat} is the catalytic constant (= V_{max}/[E]), [E] is the active site concentration, K_m is the Michaelis constant, K_{ss} is the dissociation constant of second substrate molecule bound to the peripheral anionic site (PAS) and *b*, a factor (>1) expressing the enzyme activation upon binding of second substrate molecules to the PAS. Experiments were performed in triplicate and rate data fitted with OriginPro 8.5 (Originlab Co., Northampton, MA, USA). Statistical analysis of catalytic parameters for native BChE, free labelled-enzyme and encapsulated labelled-enzyme was performed using Student *t*-test and ANOVA using OriginPro 8.5.

2.4. Enzyme titration

Labelled enzyme was titrated according to the method of Leuzinger [41] using echothiophate iodide as the titrant and BTC (1 mM) as the substrate [40]. The active site concentration of 45 U/mL preparation was 1 μM (SM Fig. S3).

2.5. Labelling of BChE with IRD probe

Human BChE was labelled with IRDye800CW NHS Ester (NIR Dye Pack, Doc #988–18,083, LI-COR Biosciences, Lincoln, NE, USA) in a reaction that covalently binds dye to lysine. In brief, 150 mg of filter-sterilized human BChE was added to 0.5 mg IRDye800CW NHS Ester. The reaction contained 25 mL of BChE in phosphate buffered saline pH 7.4 (no azide) and dye dissolved in 20 μL dimethylsulfoxide. The quantities were calculated to give equimolar amounts of IRDye800CW and BChE tetramer, with the expectation of binding 1 mol dye per 340 kDa BChE tetramer. The clear, blue-green solution was incubated in the dark at room temperature 15 h. Excess reagent was removed by dialysis against 4 L of 10 mM potassium phosphate pH 7.4 at 4 °C.

After labelling, the activity of the NIR-labelled enzyme (IRD800-BChE) was measured using the Ellman method [40]. The chemical modification did not alter the activity (see SM). The labelled enzyme was also checked by polyacrylamide slab gel electrophoresis on both native gels (after activity staining and IR fluorescence) and SDS-gels (after Coomassie Brilliant blue staining and IR fluorescence). (SM Figs. S1,2).

The BChE activity is 3178 units/mL which corresponds to 6.4 mg/ml. The labeling procedure resulted in almost no loss of activity. The ratio of IRDye800 bound per BChE tetramer was calculated according to the Li-Cor instructions for IRDye 800CW protein labelling kit (High Molecular weight, Doc#988–13,085). Because a solution of BChE tetramer at 1 mg/mL (= 2.9×10^{-6} M) has an absorbance of 1.8 at 280 nm, it follows that the extinction coefficient of BChE tetramer at 280 nm is 620,000 M^{-1} cm^{-1}. Then, the ratio of absorbance (A) of IRDye800CW-BChE at both 778 nm (A = 0.0336) and 280 nm (A = 0.2056) provided the value of 0.42 mol of IRDye800 bound per BChE tetramer. The labelled-protein was filter-sterilized into sterile vials. The IRDye800CW-BChE was frozen and stored at −20 °C.

2.6. IRD-labelled BChE loaded into polymersomes

IRD-labelled BChE (concentration ranging from 0.128 up to 0.8 mg/mL) was encapsulated into nR based on block copolymers **1a-c** polymersomes (Fig. 1). The hydrophilicity parameters (f_{PEG}) calculated as Mw(PEG)/Mw(PEG) + Mw(PPS) by comparing the integral intensity of PPS methyl group protons to that of methoxy group protons of mPEG from ^{1}H NMR spectrum are 0.23, 0.24 and 0.27 for **1a-c**, respectively. These values (<30 %) are optimal for the polymersome formation [42,43]. Triblock copolymer **1a** ($mPEG_{17}$-PPS_{34}-S-S-PPS_{34}-$mPEG_{17}$) containing a disulfide bond S-S and diblock copolymer **1c** ($mPEG_4PPS_{70}$-Bn) without a disulfide bond were synthesized by methods described in our previous works [26,27].

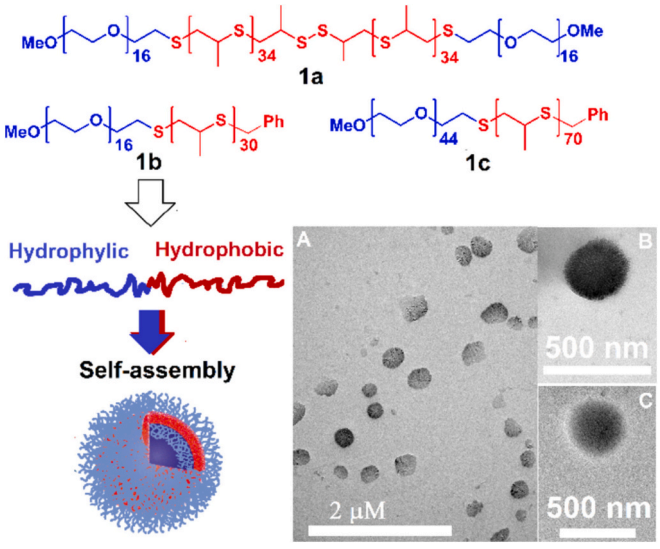

Fig. 1. Structures of tri- and di-block copolymers **1a, 1b** and **1c** (S is sulfur atom) and TEM imaging of empty polymersomes based on **1b**, $C_{\mathbf{1b}}$ = 0.05 μg/mL, Tris buffer, pH = 7.4, 25 °C. Scale bar is 2 μm (A) and 500 nm (B, C), in the presence (A, B) and absence (C) colloid Ag.

2.6.1. Synthesis of amphiphilic block-copolymers *1b*

Synthesis of the $mPEG_{17}$-PPS_{30}Bn polymer was carried out in accordance with Scheme 1. To synthesize **1b** based on polyethylene glycol monomethyl ether $mPEG_{17}$-OH, we chose the route using mesylate $mPEG_{17}$-Ms. For this purpose, mesylation of $mPEG_{17}$-OH was performed [44] and described in detail in SM. Mesylate $mPEG_{17}$-Ms was treated with an excess of potassium thioacetate in DMF to obtain thioacetate $mPEG_{17}$-SAc. Then, DMF was removed on rotary evaporator, the residue was extracted with CH_2Cl_2, washed with water, dried over Na_2SO_4, and after removing the solvent, dried in vacuum.

Next step was carried out, using slightly modified *one pot* method [45], detailed in SM. **1b** was obtained as a light brown oil. The structure of **1b** was confirmed, using ^{1}H NMR and ^{13}C (SM, Figs. S4–S6). The ratio of units was determined by integrating the signals in ^{1}H NMR spectra (SM), using as a reference point the singlet of the terminal methoxy group, which is clearly visible and appears separately from other signals. The signal of the methylene group, a multiplet with a shift about 3.8 ppm, was integrated. It was a control of benzylation completeness of the terminal sulfhydryl group.

$mPEG_{17}$-Ms Light-brown powder. Yield 96 %. ^{1}H NMR (600 MHz, $CDCl_3$) *δ*: 4.37 (m, 2H, O-CH_2<u>CH_2</u>OSO_2), 3.76 (m, 2H, O-<u>CH_2</u>CH_2OSO_2), 3.69–3.60 (m, 63H, CH_2 broad, PEG chain protons), 3.54 (m, *J* = 5.8, 3.6 Hz, 2H), 3.37 (s, 3H, CH_3O), 3.08 (s, 3H, CH_3SO_2).

$mPEGS_{17}$_Ac Brown oil. Yield 77 %. ^{1}H NMR (600 MHz, $CDCl_3$, 30 °C) *δ*: 3.68–3.63 (m, 73H, CH_2 broad, PEG chain protons), 3.58–3.55 (m, 2H, -O<u>CH_2</u>CH_2S-), 3.39 (s, 3H, CH_3O), 3.11 (t, *J* = 6.4 Hz, 2H, -<u>CH_2</u>$SCOCH_3$), 2.37 (s, 3H, $CH_3C(O)S$).

$mPEG_{17}$-PPS_{30}_Bn ^{1}H NMR (400 MHz, $CDCl_3$) *δ*: 7.33–7.26 (m, 4H, PhH), 7.24–7.19 (m, 1H, PhH), 3.77 (brs, 2H, <u>CH_2</u>Ph), 3.66–3.59 (m, 68H, <u>broad, PEG chain protons</u>), 3.52 (dd, *J* = 5.8, 3.5 Hz, 2H, O<u>CH_2</u>CH_2S), 3.36 (s, 3H, OCH_3), 2.96–2.81 (m, 60H, CH_2 (PPS)), 2.66–2.55 (m, 30H, CH (PPS)), 1.37–1.33 (m, 90H, CH_3 (PPS)). ^{13}C NMR (101 MHz, $CDCl_3$) *δ*: 138.37 (s, *i*-Ph), 128.88 (s, *m*-Ph), 128.64 (s, *o*-Ph), 127.14 (s, *p*-Ph), 72.02 (s, O**<u>CH_2</u>**CH_2S), 71.18 (s, **<u>CH_2</u>**OCH_3), 70.62 (s, CH_2 (PEG)), 59.11 (s, OCH_3), 41.41 (s, CH (PPS)), 41.33 (s, CH (PPS)), 38.56 (s, CH_2 (PPS)), 38.50 (s, CH_2 (PPS)), 38.46 (s, CH_2 (PPS)), 35.63 (s, **<u>CH_2</u>**Ph), 32.55 (s, OCH_2**<u>CH_2</u>**S), 20.84 (s, CH_3 (PPS)). FT-IR 3420, 2958, 2884, 2740, 2695, 1467, 1453, 1415, 1373, 1361, 1343, 1280, 1234, 1174, 1148, 1112, 1061, 1002, 963, 947, 844, 734, 690, 530.

2.6.2. Preparation of empty and IRD-labelled BChE-loaded polymersomes

Slightly modified thin-film hydration method was used for preparation of polymersomes [26]. Block copolymers **1a-1c** (0.1–1 % *w*/w) were dissolved in 1 mL ethanol:chloroform (1,1). The homogeneous polymer solution was kept during 3 h at 34 °C for preparing the thin film and then overnight for alcohol evaporation. Pre-heated (37 °C) Tris-buffer (10 mM, pH 7.4) was added to rehydrate the thin-film of block copolymers in the absence or presence of IRD-labelled BChE. The solution was stirred under magnetic stirring (600 rpm) (Ika, Germany) for 3 h at 37 °C, and then, overnight at room temperature.

2.6.3. Physico-chemical characteristics

Mean particle size, zeta potential and polydispersity index were determined by dynamic light scattering (DLS), using a Malvern Instrument Zetasizer Nano (Worcestershire, UK) and Brookhaven 90Plus Nanoparticle Size Analyzer (Holtsville, New York, USA). The size (hydrodynamic diameter, nm) was calculated according to the Einstein–Stokes relationship, $D = k_BT/3\pi\eta x$, in which *D* is the diffusion coefficient, k_B is the Boltzmann's constant, *T* is the absolute temperature,

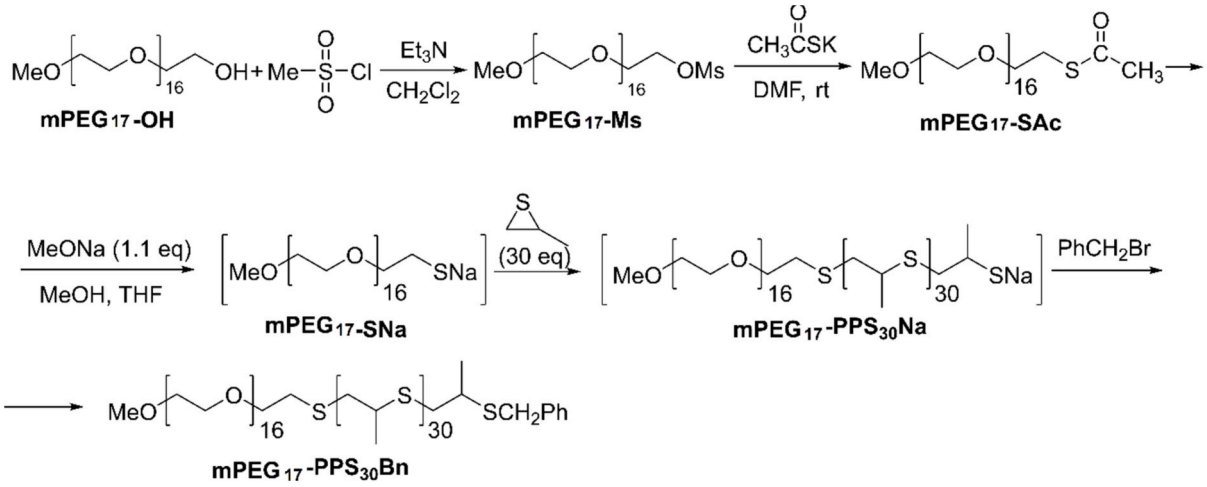

Scheme 1. Synthesis of PEG-PPS di-block copolymer **1b**.

η is the viscosity, and x is the average hydrodynamic diameter of nanoparticles. The diffusion coefficient was determined for each sample. All samples were analyzed in triplicate.

Transmission electron microscopy (TEM) was used to image the size and to reveal the morphology of both empty and IRD-labelled BChE-loaded into polymersomes. TEM images were obtained, using a Hitachi HT7700 (Exalens microscope, Japan). The images were acquired at an accelerating voltage of 100 keV. Samples (Cpolym = 0.05 μg/mL) were added to a 300-mesh copper grid with continuous carbonformvar support films.

Encapsulation efficiency (EE, %) and loading capacity (LC, %) were assessed for samples containing IRD-labelled BChE. These parameters were determined indirectly by filtration/centrifugation, measuring the free enzyme concentration by spectrophotometry. A volume 500 μL of each BChE-loaded polymersome was placed in a centrifugal filter device Vivaspin 500 Centrifugal Concentrator, 1000 kDa (Sartorius Stedim Biotech GmBH, Goettingen, Germany) to separate polymersomes and aqueous phases and centrifuged at 3000 rpm and 25 °C for 5 min, using a centrifuge (Eppendorf SE, Germany). The concentration of free IRD-labelled enzyme in Tris buffer was quantified by absorbance using Perkin Elmer λ_{35} (Perkin Elmer Instruments, USA) at 778 nm (ε = 97,869 M^{-1} cm^{-1} in 10 mM Tris buffer, pH = 7.4). UV absorbance spectra and calibration curve are presented in file (SM, Fig. S7). Encapsulation parameters, *EE*% and *LC*%, (Eqs. (2), (3)), were calculated against appropriate calibration curve, using the following equations:

$$EE(\%) = \frac{Total\ amount\ of\ enzyme - Free\ enzyme}{Total\ amount\ of\ enzyme} \times 100\%, \quad (2)$$

$$LC(\%) = \frac{Total\ amount\ of\ enzyme - Free\ enzyme}{Total\ amount\ of\ copolymer} \times 100\%, \quad (3)$$

2.6.4. Purification of IRD-labelled BChE-loaded polymersomes

To remove non-encapsulated enzyme, the filtration/centrifugation method was implemented using centrifugal filter devices Vivaspin 500 Centrifugal Concentrator, 1000 kDa (Sartorius Stedim Biotech GmBH, Goettingen, Germany). Fractions of 0.5 mL were centrifuged at 3000 rpm 4 °C for 5 min, using Eppendorf centrifuge 5702 (Eppendorf SE, Germany) using the conditions of our previous work [26]. These conditions were determined by monitoring the transmittance of empty polymersomes under the same centrifugation conditions over time. The same amounts of empty polymersomes were transferred to micro-centrifuge tubes, and after centrifugation the turbidity was measured. Transmittance of empty polymersomes is shown in SM, Fig. S8.

2.6.5. Release of IRD-labelled BChE from polymersomes

Monitoring of IRD-labelled BChE release from polymersomes was performed using the dialysis bag diffusion method. The spectra/Por® Dialysis membrane (Biotech CE Tubing, MWCO: 1000 kDa) were soaked in Milli-Q water for 48 h before use. 1 mL IRD-labelled BChE-loaded nanoreactors were poured into dialysis membranes. The two bag ends were sealed with clamps. The bags were then placed in a vessel containing 10 mL of 10 mM Tris buffer, pH 7.4, the receiving phase. The vessels were placed in a thermostatic shaker at 25 °C, under a stirring rate of 150 rpm. At predetermined time-intervals, 0.6 mL samples were taken to measure the absorbance at 778 nm (ε = 97,869 M^{-1} cm^{-1} in 10 mM Tris buffer, pH = 7.4), using a Perkin Elmer λ_{35} spectrophotometer (Perkin Elmer Instruments, USA).

2.7. Animal studies

Mice-CD-1 (males, 6–10 weeks, 20–25 g) were used for the experiment. They were maintained under standard conditions (12 h light/dark cycle, 22 ± 3 °C and a 50 ± 20 % relative humidity). The adaptation time before starting experiment was at least 10 days. During this period, daily inspection of external animal conditions was carried out. All experimental procedures with animals were performed in accordance with the Ethical Principles in Animal Research and were approved by the Local Ethics Committee of the Kazan Federal University (protocol №40).

3 groups were formed by random selection, using body weight as a leading sign (the spread in initial weight between and within groups was ±20 %). Animals were not fed overnight before the experiment to minimize possible auto-fluorescence. The hair of mice was removed before the experiment, using a depilatory gel. To ensure immobility during experiment, animals were under anesthesia with Zoletil®100 (Laboratoires Virbac, France). The free IRD-labelled enzyme solution, IRD-labelled enzyme-loaded into polymersome solution, and control (0.9 % *w*/w NaCl) were injected into the tail vein. Fluorescence imaging of entire animals and selected organs showing fluorescence (liver, stomach, whole intestine, kidneys, lungs, heart, spleen, urine bladder) was carried out after 10 min, 30 min, 1, 2, 3, 4 h and daily for 7 days on an IVIS Spectrum Imaging System. After each experimental point, blood was collected into plastic tubes with heparin for pharmacokinetic study.

2.7.1. Pharmacokinetics

Free enzyme and enzyme nanoreactors were intravenously injected (*i.v*) to the tail vein at time 0 (t_0). Blood samples, 0.5 mL, were taken in each animal at different times on heparinized tubes and immediately centrifuged (15 min at 5000 rpm) to separate plasma from blood cells.

Animals were euthanized after taking blood at each time point. The decay in BChE activity in plasma was monitored as a function of times t up to 7 days after injection. BChE activity was assayed using the Ellman method. Pharmacokinetic data were analyzed using compartmental and non-compartmental approaches. The simple two-compartment open model for intravenous bolus injections was used. Accordingly, the first-order process of BChE decay obeys Eq. (4), where E_t is the enzyme activity at time t after, E_0 is the extrapolated initial value of enzyme activity in plasma at t_o, α the rate constant for distribution (d) with half-time of distribution (Eq. (5)), and β the rate constant of enzyme elimination (el) from the blood compartment. The half-time of elimination is in Eq. (6).

$$E_t = E_0 e^{-\alpha t} + (E_0 - B) e^{-\beta t} \quad (4)$$

$$t_{1/2,d} = Ln2/\alpha \quad (5)$$

$$t_{1/2,el} = Ln2/\beta \quad (6)$$

For the non-compartmental analysis, plots corresponding to Eq. (4) allowed to determine areas under the curve (AUC). Then, areas under the first moment curve (AUMC) were determined by plotting $E_t.t$ *vs* time. The mean residence times (MRT) were calculated from ratios AUMC/AUC, and rate of enzyme elimination from the bloodstream, k_{elim}: 1/MRT.

2.7.2. *In vivo, ex vivo imaging and biodistribution studies of free IRD-labelled enzyme and enzyme encapsulated into polymersomes*

Mice under anesthesia were fluorescently imaged using the following excitation and emission filters 745 nm and 840 nm respectively. Epi-fluorescent images were acquired on an IVIS Spectrum Imaging System (Perkin Elmer, Santa Clara, USA) at 0.167, 0.5, 1, 2, 3, 4 h, and then, 1, 2, 3, 4, 5 and 7 days post-administration. Following *in vivo* imaging, mice were humanely killed, the organs were excised and then fluorescently imaged, using the IVIS Spectrum (using the above-mentioned filter) for *ex vivo* study. To standardize the study, all images were acquired under the same field of view using exposure time 1, which corresponded to pixel binning of 8 and f/Stop of 2. Data were analyzed using Living Image. The signal to background ratio was calculated by evaluating the radiance in the region of interest (liver and bladder area *in vivo* or liver and stomach area *ex vivo*). We report ROI values as "Average Radiant Efficiency" [p/s/cm^2/sr]/[μW/cm^2] (=Radiant Efficiency/ROI surface area).

3. Results

3.1. *Characteristics of empty and IRD-labelled enzyme-loaded polymersomes*

The morphology of empty polymersomes prepared by thin film hydration method, using block copolymer **1b** is shown in Figs. 1 and S9. Silver colloid nanoparticles were used as a contrast agent for electron microscopy analysis. Spherical monomeric nanoparticles with a size close to 200 nm are shown in Fig. 1.

The sizes of empty nR observed by TEM are close to the data obtained by DLS (Table 1). The structure of block copolymers affects the size of polymersomes. It can be seen from data in Table 1 that the diameter of empty polymersomes increases in this row **1c** < **1a** < **1b**, according to the presence of PEG on respective units. Polydispersity index for all nanosystems is almost the same and it is not higher than 0.2. The zeta potential of **1b** polymersomes is around -6 mV, that is close to the value of diblock copolymer **1c** but lower than for triblock copolymer **1a** (−12 mV).

The next step was the encapsulation of enzyme into polymersomes. The **1b** copolymer concentration varied from 1 to 10 mg/mL (SM, Fig. S10) and the enzyme concentration ranged from 0.128 to 0.8 mg/mL (SM, Fig. S11). Table 1 and SM figures show that the characteristics of enzyme-loaded polymersomes (size, zeta potential, polydispersity) did not change with variation of polymer and enzyme concentrations. The optimal polymer concentration for the stability was 5 mg/mL The enzyme-loaded polymersomes have good colloid stability over >1 year. The excellent encapsulation efficiency (EE%) slightly improved with increasing the polymer concentration from 84 ± 5 % (C = 1 mg/mL) to 93 ± 3 % (C = 10 mg/mL). UV Absorbance spectra of enzyme for determination of EE% are presented in SM Fig. S12. Then, we increased the enzyme loading capacity (LC%) to 6 % by increasing the enzyme concentration. Polymersomes based **1b** with C = 1 mg/mL has a good LC =11 ± 0.6 %, but EE was only 84 ± 5 % and stability was not good. To compare polymersomes with different polymer structures, we chose an optimal polymer concentration of 5 mg/mL and an enzyme concentration of 0.32 mg/mL. TEM pictures of enzyme-loaded polymersomes

Table 1
Dynamic light scattering data for empty and *IRD-labelled* BChE-loaded polymersomes in 10 mM Tris buffer, pH = 7.4, 25 °C; size is hydrodynamic diameter, *Z*-average is the mean size, PDI is polydispersity index, ξ or zeta potential is electrokinetic potential.

bl-copolymer	Conc/polym (mg/mL)	Conc. Enz. (mg/mL)	Size (nm)		Z-aver (nm)	PDI	ξ (mV)	EE, (%)	LC, (%)
			Int	Num					
1a[a]	5	–	122 ± 18	68 ± 15	114 ± 1	0.11 ± 0.01	−12 ± 1	–	–
1b	5	–	142 ± 20	68 ± 13	130 ± 5	0.15 ± 0.01	−5 ± 2	–	–
1c[b]	5	–	106 ± 13	44 ± 10	94 ± 2	0.17 ± 0.01	−6.5 ± 0.3	–	–
1b	1	0.128	142 ± 12	60 ± 13	135 ± 2	0.27 ± 0.01	−9.4 ± 0.3	84 ± 5	11 ± 0.6
1b	2	0.128	142 ± 17	60 ± 12	130 ± 2	0.21 ± 0.01	−4 ± 3	–	–
1b	5	0.128	142 ± 20	68 ± 14	135 ± 2	0.2 ± 0.01	−6 ± 1	87 ± 7	2.2 ± 0.2
1b[c]	5	0.128	142 ± 17	68 ± 13	133 ± 1	0.18 ± 0.01	−6 ± 1	–	–
1b	10	0.128	142 ± 20	79 ± 17	149 ± 2	0.17 ± 0.01	−5 ± 1	93 ± 3	1.1 ± 0.04
1b	5	0.213	164 ± 20	68 ± 15	135 ± 2	0.16 ± 0.01	−7 ± 1.0	90 ± 6	3.8 ± 0.3
1b	5	0.256	142 ± 17	68 ± 15	138 ± 2	0.18 ± 0.01	−6 ± 1	90 ± 7	4.6 ± 0.4
1b[d]	5	0.256	142 ± 17	68 ± 15	145 ± 2	0.22 ± 0.02	−6 ± 1	–	–
1b	5	0.32	142 ± 16	68 ± 12	138 ± 1	0.2 ± 0.01	−6 ± 1	94 ± 7	6 ± 0.5
1b[e]	5	0.32	142 ± 16	68 ± 12	137 ± 6	0.23 ± 0.01	−5 ± 1	–	–
1b	5	0.8	142 ± 21	79 ± 17	134 ± 5	0.11 ± 0.02	−6 ± 1	–	–
1a	5	0.32	122 ± 16	68 ± 16	126 ± 1	0.2 ± 0.01	−16 ± 7	83 ± 7	5.3 ± 0.5
1c	5	0.32	106 ± 13	51 ± 12	109 ± 1	0.16 ± 0.01	−5 ± 0.4	91 ± 4	5.8 ± 0.3

[a] [26].
[b] [27].
[c] Stability during 2 months at 4 °C.
[d] Stability during 1 year at 4 °C.
[e] Stability during 6 months at 4 °C.

based on **1a**, **1b** and **1c** polymers are shown on Fig. 2. As can be seen, the size of polymersomes **1b** is larger than **1a** and **1c**. This is consistent with DLS data presented in Table 1. The EE% enzyme in **1b** polymersomes is higher than for **1a** and **1c** polymersomes.

The release of enzyme from polymersomes was monitored by spectrophotometry at λ = 778 nm (SM, Fig. S13) for fluorescent BChE that had crossed the 1,000,000 MW cut off dialysis membrane. Complete burst release took >8 h for the encapsulated enzyme compared to the free enzyme (about 90 min for 90 % release). For the free enzyme, there was almost no more increase in release up to 290 min, and the experiment was discontinued after this time (Fig. 3). This burst release can be explained by several mechanisms [46–49]. We still do not know which mechanisms account for release of BChE from polymersomes.

3.2. Kinetic studies of free and IRD-labelled enzyme loaded into polymersomes

The enzyme activity was monitored in buffer (Fig. 4A) and then in blood (Fig. 4B) with BTC as the substrate.

To evaluate the effect of labelling and encapsulation on enzyme activity, the catalytic parameters of free BChE and BChE-loaded into polymersomes were determined (Table 2, Fig. 4A). Kinetics curves of BTC hydrolysis by free IRD-labelled BChE and IRD-labelled BChE-loaded into polymersomes are shown in Figs. S14 and S15. According to Table 2 data neither the covalent labelling of enzyme with NIR probe nor the encapsulation of enzyme dramatically altered the catalytic properties of BChE.

Catalytic parameters of free, IRD-labelled and encapsulated IRD-labelled BChE are similar. Student t-test and ANOVA (Figs. S16–S20) show that there is a slight difference in K_{ss} that could be explained by a mild alteration of the protein molecular dynamics caused by covalent binding of the fluorescent probe on enzyme surface. However, K_{ss} values for the labelled enzyme are mildly altered. This indicates that binding of the second substrate molecule on the peripheral anionic site (PAS) is not impaired by the presence of the probe on enzyme surface. Moreover, taking into account that encapsulated BChE must display a high bimolecular rate constant for fast reaction with OPs, the fact that the bimolecular rate constant (k_{cat}/K_m) for BTC as the model substrate, is not altered compared to free enzyme behavior, it can be stated that the reactivity of encapsulated enzyme with OPs will be similar to that of free enzyme. Thus, polymersome encapsulation does not alter the functional properties of the enzyme.

Since the process of preparing plasma for pharmacokinetic studies includes a centrifugation step of blood, it was necessary to study the enzyme activity in plasma during centrifugation. Indeed, owing to the size of nR, the sedimentation rate of free and encapsulated enzyme could be different. Kinetic dependencies are in SM Fig. S21. As we see in Fig. 4B, the activity of enzyme-loaded into polymersomes decreased 2 times during 15 min centrifugation (2500 rpm). The polymersomes sedimented during 15 min so that less encapsulated enzyme activity remained in the upper part of plasma compared to centrifuged free enzyme. Such a sedimentation was also observed in buffer when the conditions were selected for determination of encapsulation efficiency. The rate of sedimentation of nanoparticles in buffer (or injectable medium) is an important issue that determines homogeneity of administered doses of E-nR. Future directions of research have to focus on engineering the dilution medium (e.g by adding additives) to get stable and homogenous preparations of E-nR.

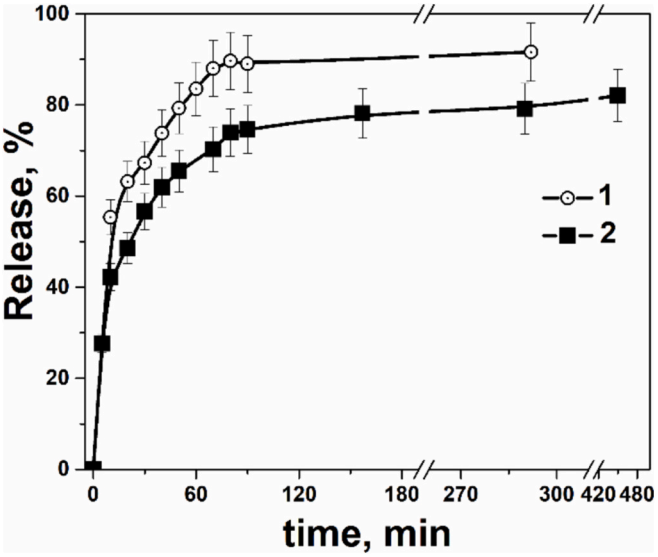

Fig. 3. Enzyme release from dialysis bag: 1-control (free IRD-labelled enzyme), 2- IRD-labelled BChE-loaded polymersomes, C_{1b} = 5 mg/mL, Cenzyme = 0.32 mg/mL, in 10 mM Tris buffer, pH 7.4, 25 °C.

3.3. Pharmacokinetics

The pharmacokinetics of BChE in animal plasma was monitored up to 7 days after injection. A study of the kinetics of activity over time is presented in the Figs. S22 and S23. Decay of BChE activity in plasma revealed similar profiles for injected free enzyme and encapsulated enzyme (Fig. 5).

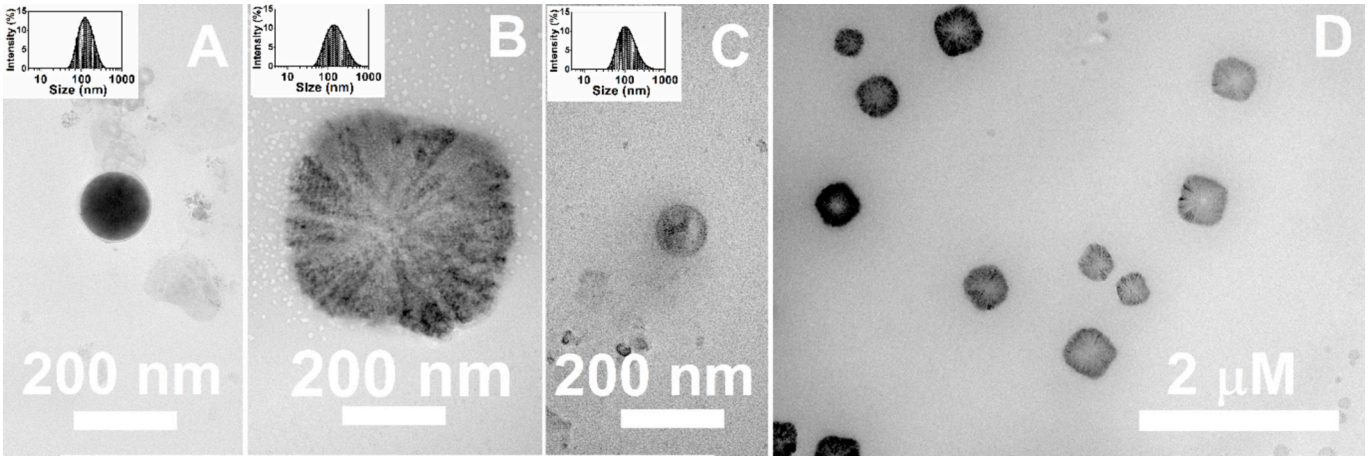

Fig. 2. TEM imaging and DLS distribution of IRD-labelled BChE loaded-polymersomes based on **1a** (A), **1b** (B, D) and **1c** (C), Cpolymers = 0.05 μg/mL, Tris-Buffer, pH = 7.4, 25 °C. Scale bar is 200 nm (A–C) and 2 μm (D).

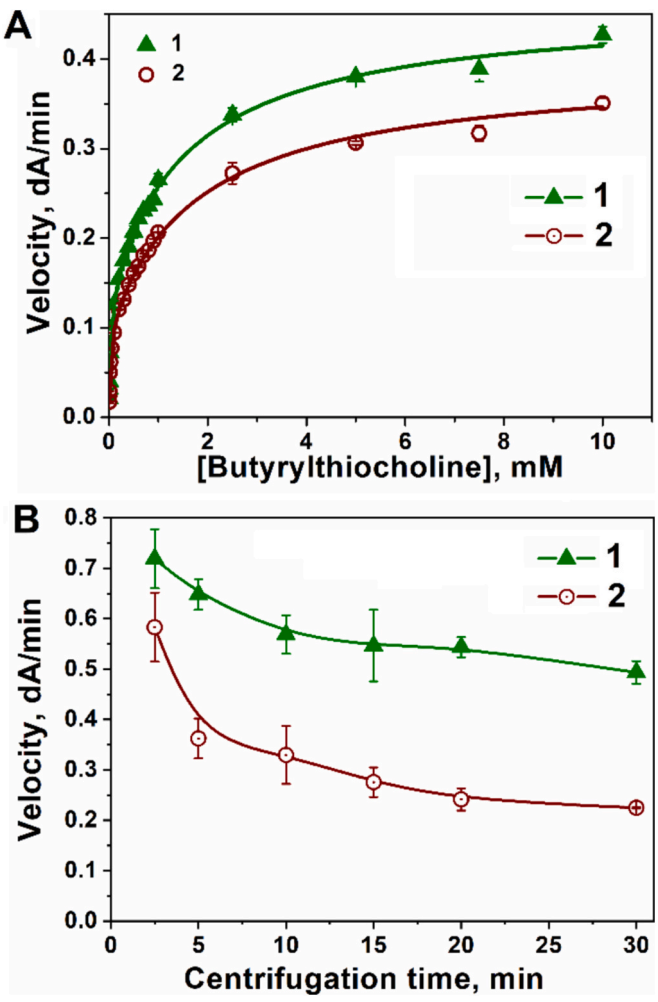

Fig. 4. Dependence of initial rates of butyrylthiocholine hydrolysis by free IRD-labelled BChE (1) and IRD-labelled BChE-loaded into polymersomes (2) on BTC concentration in phosphate buffer 0.1 M, pH 7.0, C_{BChE} = 0.4 nM (A) and in plasma as a function of the centrifugation time of blood at 2500 rpm, C_{BChE} = 0.4 nM, (B) 25 °C.

Table 2
Catalytic parameters (±SE) for BChE-catalyzed hydrolysis of BTC in phosphate buffer, 0.1 M, pH 7.0, 25 °C.

Catalytic parameters	BChE	IRD-labelled BChE	IRD-labelled BChE-loaded into polymersomes
k_{cat} (min^{-1})	23,500 ± 950	26,800 ± 300	20,000 ± 400
K_m (μM)	18 ± 3	26 ± 1	23 ± 1
k_{cat}/K_m x 10^{-9} (M^{-1} min^{-1})	1.3 ± 0.2	1.03 ± 0.5	0.87 ± 0.05
K_{ss} (μM)	1260 ± 230	1570 ± 100	1800 ± 170
b	3.6 ± 0.2	3.2 ± 0.1	3.7 ± 0.2

It is important to note that the injected dose of free enzyme and enzyme-loaded polymersomes was identical in terms of enzyme activity. Yet, PK profiles show different ordinates (activity extrapolated at $t = 0$), *i.e.* lower activity for encapsulated enzyme. These apparent activity decays are artefactual. In fact, the lower activity of encapsulated enzyme compared to free enzyme results from partial sedimentation of enzyme-loaded polymersomes during centrifugation of heparinized blood. The longer the centrifugation time at constant rotation speed (rpm), the lower the encapsulated activity in the centrifuged plasma upper phase (see Fig. 4B and SM, Fig. S21). Enzyme nanoreactors as nanoparticles, co-sediment with red and white blood cells, because their large size/mass compared to free enzyme. Pharmacokinetic parameters are in Table 3. As we can see, compartmental analysis shows that the distribution and elimination phases are clearly prolonged using polymersomes by 2.7 times and 2 times, respectively. However, non-compartmental analysis shows that MRT is not significantly increased in case of *E*-nR.

At each time-point animals were scanned for IRD fluorescence analysis. Real time distribution of IR fluorescence in organs was monitored up to 7 days (Fig. 5C). The presence of NIR fluorescence was mainly detected in liver shortly after injection (SM, Fig. S24). NIR fluorescence was also detected in urine bladder (SM Fig. S25). There was no presence of NIR-BChE in the brain and other organs. This fits with previous reported results with injected horse BChE in rodents [35,36]. This confirms that enzyme alone or in nanoreactor cannot cross the blood brain barrier, and that unlike block inomer complex used for encapsulation of horse BChE [17], our enzyme nanoreactor cannot open to deliver BChE into the brain.

3.4. IRD-labelled BChE distribution in organs

After fluorescence imaging animals were euthanized. Organs were collected *post mortem* and individually analyzed for IRD fluorescence. Both control and experimental animals showed fluorescence in stomach *ex vivo* throughout the experiment. There was no significant difference when comparing signal levels between experimental animals and controls. This allows us to assume that in all samples the stomach glow was autofluorescence due to diet. Fluorescence was observed *ex vivo* in the liver 10 min after administration of both free BChE and BChE-loaded into polymersomes (Fig. 6). No fluorescence was observed in control mice. Interestingly, the level of fluorescence intensity *ex vivo* in liver does not correspond to the level of the signal obtained in the same time periods *in vivo*. *Ex vivo* liver fluorescence reached maximum at 3 h for free BChE. Unlike free BChE, for BChE-loaded into polymersomes we see almost plateau until 48 h. In addition, the level of fluorescence at 3 and 4 h for free BChE was significantly higher than for the fluorescence of BChE-loaded into polymersomes that showed no peak of intensity.

The enzyme was eliminated by the liver, and then fluorescence was found in intestine and feces. It must be noted that fluorescence appeared in the urine bladder after several hours (maximum fluorescence between 4 and 24 h). However, it is unlikely that elimination of intact enzyme by kidney took place. Thus, the presence of fluorescence in urine was puzzling because no fluorescence was detected in kidney. A plausible hypothesis was that IRD labelled-BChE, partly degraded in the liver, was clipped by different proteases in the intestine, and then, resulting polypeptides and amino-acid fragments, partially re-absorbed in blood, were subsequently filtered by the kidney.

4. Discussion

Simple preparation conditions (involving neither heating, nor organic solvents, extrusion, and sonication step) were used for encapsulation of IRD-labelled BChE. The soft process we used prevented enzyme inactivation inside polymersomes. It was showed the encapsulation did not alter the functional properties of the enzyme with BTC as model substrate. In addition, under our conditions, the size of nanoparticles, about 140 nm, is suitable for intravenous administration. It should be noted that the loading characteristics (EE and LC) quite high are good: 94 and 6 %, compared to available literature data for BChE in liposomes (in the range of 30–50 %) [15,16] and other proteins [50].

Compartmental analysis showed that the half-time for distribution of injected free IRD-labelled BChE and encapsulated IRD-labelled enzyme was 6.64 ± 2.72 and 17.64 ± 3.5 h, and the half-time for elimination was 72.20 ± 9.4 h and 150.7 ± 67.8 h, respectively. However, non-compartmental analysis showed that MRT values were of the same

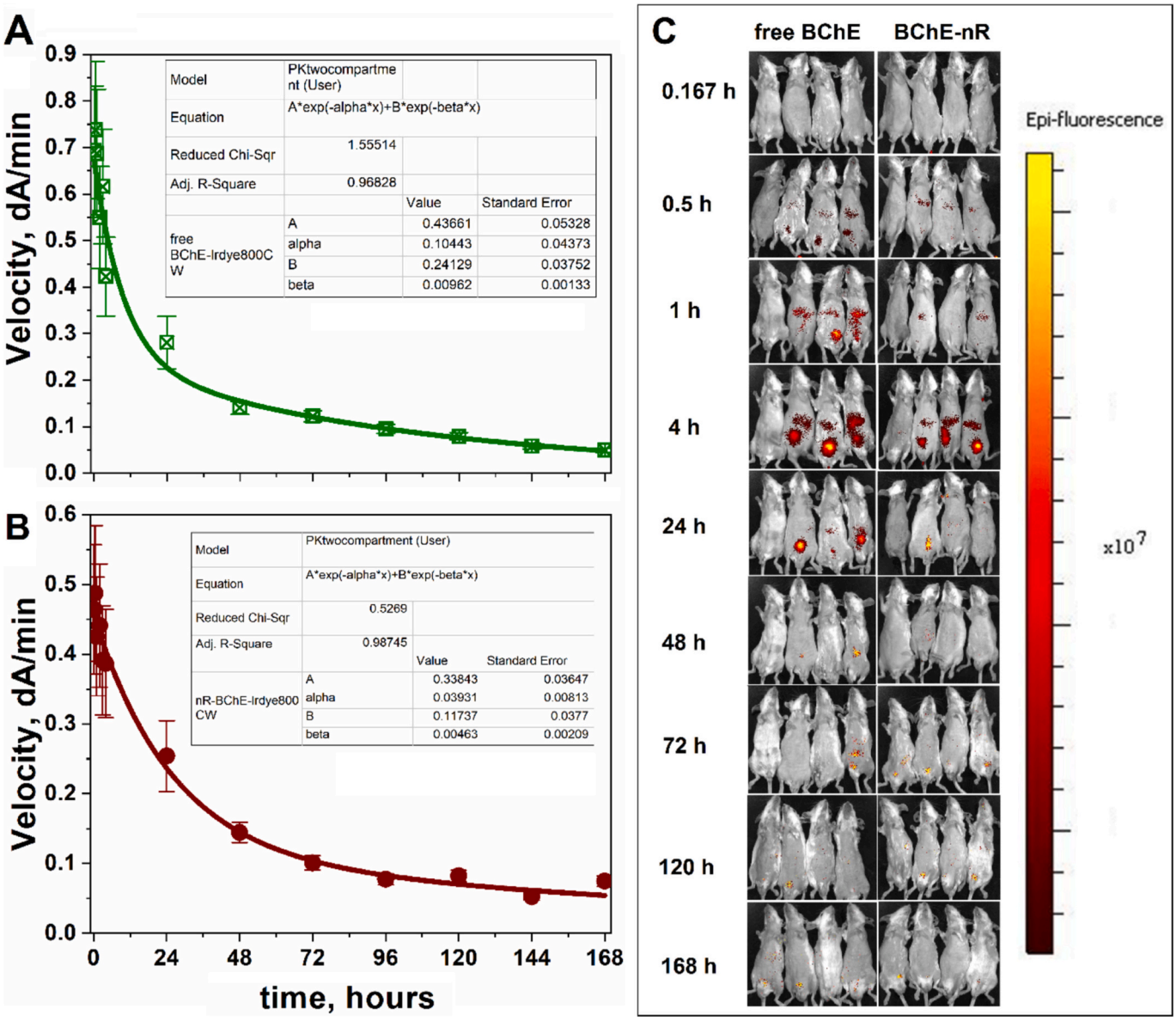

Fig. 5. PK of elimination of free IRD-labelled enzyme (A) and IRD-labelled enzyme-loaded polymersomes (B) from mouse blood, Real-time biodistribution analysis (C), (*bolus* injection in tail vein), the dose of enzyme 1.5 mg/kg, the dose of PEG-PPS polymersomes 25 mg/kg.

Table 3
Pharmacokinetic parameters for *i.v* injected free IRD-labelled BChE enzyme and IRD-labelled enzyme-loaded into polymersomes, in mice, dose of enzyme 1.5 mg/kg.

	$t_{1/2,d}$ (h)	$t_{1/2,el}$ (h)	α (h^{-1})	β (h^{-1})	MRT (h)	k_{elim} (h^{-1})
Free E	6.6 ± 2.7	72.20 ± 9.4	0.10 ± 0.04	0.01 ± 0.001	51.2 ± 13.50	0.019 ± 0.005
E-nR	17.6 ± 3.5	150.7 ± 67.8	0.039 ± 0.008	0.005 ± 0.002	54.1 ± 14.11	0.02 ± 0.005

order for both enzyme preparations, about 50 h. First, about PK of the free enzyme, previously reported results showed that MRT of injected human BChE tetramer to mice, regardless of the dose and route of administration, is close to 50 h [51,52]. Compartmental PK analysis showing that IRD-labelled BChE was eliminated with $t_{1/2}$ = 72 h is in agreement with previously reported half-time for injected IRD-labelled and free horse BChE in mice (67 h *vs* 30 h) [35]. This indicates that the presence of the covalently-linked probe on the enzyme surface affected PK, prolonging residence time of the IRD-labelled BChE in blood. At this point we also should mention that IRD800-labelling slightly affected the substrate binding properties of the enzyme (binding on surface PAS), but did not impair the catalytic machinery of the enzyme.

However, it should be mentioned that one cannot strictly compare PK of free molecules, including proteins, with PK of nanomaterials. For PK of nanomaterials, the terms, distribution phase and elimination phase, have become obsolete in precisely delineating biphasic clearance of nanomaterials/drug delivery systems [53]. The proposed new terms are α-phase for the interaction/saturation phase (sharp) and β-phase for the RES clearance phase (slow). More than half of nanomaterials have a sharp α-phase, including landmark nanomedicine products (Doxil and Abraxane). The obtained value for BCh*E*-nR, $t_{1/2}$–18 h, is close to literature data, 10–20 h, for PEG polymers [54,55], but higher than for stealth liposomes [56,57]. Formation of a protein corona on PEGylated

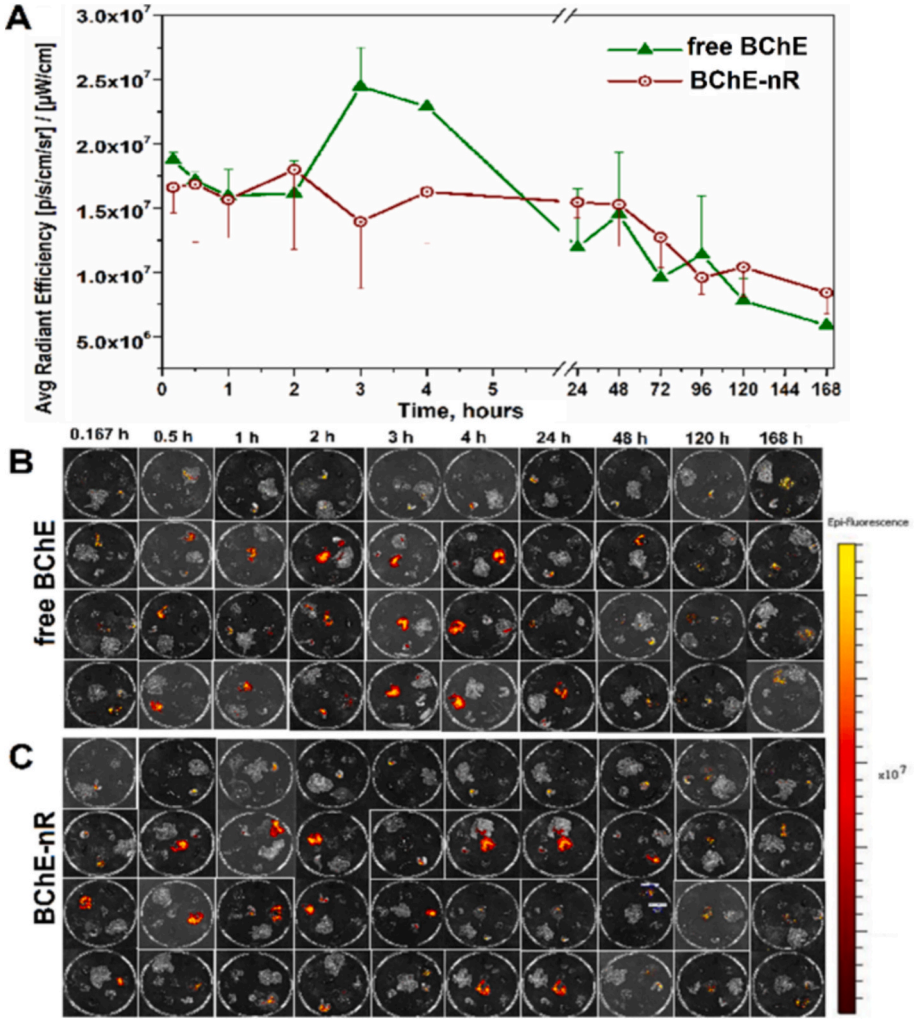

Fig. 6. Time biodistribution analysis of *ex vivo* NIR fluorescence in the liver after *iv* administration of free IRD-labelled BChE (B) and IRD-labelled BChE-loaded into polymersomes (C). The enzyme dose was 1.5 mg/kg, the dose of PEG-PPS polymersomes was 25 mg/kg, 3 animals per time point and 1 animal-control (top row). The multiple fragments in panels B and C are the different organs taken at each time-point.

liposomes is a key to increase their residence time in the circulation [58], while for PEG-polymersomes, prolonged circulation occurred without a significant amount of plasma proteins associated with their surface. Typically after intravenous administration most nanoparticles accumulate in the liver and spleen [54,59] by interacting with phagocytes in these organs.

Another important point about the elimination PK of E-nR by the liver is the contrast with free enzyme. Whereas the rate of elimination of free enzyme is maximal at 3 to 4 h, the rate of elimination of E-nR has no peaks (Fig. 6A). While elimination of free glycoproteins like BChE involves endocytosis after binding on specific hepatocyte surface receptors in liver, the uptake and elimination of nanomaterials involves continuous and highly effective phagocytosis by macrophages, Kupfer cells and liver sinusoidal endothelial cells, delaying interactions with hepatocytes and hepatobiliary elimination [60–63]. Thus, free and encapsulated enzymes are eliminated *via* different pathways.

5. Conclusion

The enzyme nanoreactor approach is conceptually of paramount importance for fast elimination of toxic molecules in the body. It allows the use of highly concentrated fast-reactive enzymes, operating in narrow confined space and performing catalytic reaction under second-order conditions [64]. Our approach of human BChE showed the functional properties of the enzyme are not altered by encapsulation in nanoreactors. However, the nanobiotechnology of enzyme nanoreactors is still in infancy and there is a lack of information about *in vivo* operational stability of these nanobodies, including PK and elimination. In particular, until recently, the mechanisms of recognition and elimination of polymeric envelopes was poorly documented. In this work, the use of the NIR approach for labelling BChE allowed to monitor organ distribution and elimination path of free BChE and encapsulated BChE after injection in mice. It was found in particular that enzyme nanoreactors can be continuously eliminated by the liver. Therefore, for the future, enzyme nanoreactor technology has to pay attention to this issue. To improve the efficiency of enzyme nanoreactors compared to free bioscavenging enzymes, the residence time of injected nanobodies has to be significantly increased. Several strategies can be implemented. Double envelope technology, using encapsulated enzymes in stable polymeric membrane and over-encapsulation of these nanobodies into red blood cell ghosts or in decorated polymeric envelopes compatible with the reticulo-endothelial system are appealing approaches that have been successfully applied for other proteins and enzyme systems [65–67]. Works are in progress in our laboratory to develop this strategy. Thus, this work initiates new research on novel formulation of BChE-based encapsulated bioscavengers, *i.e.* nanoreactors containing a high concentration of enzyme, aimed at increasing the residence time of functional OP-reacting enzymes in the blood stream.

CRediT authorship contribution statement

Tatiana Pashirova: Writing – original draft, Methodology, Investigation, Conceptualization. **Zukhra Shaihutdinova:** Investigation. **Dmitry Tatarinov:** Investigation. **Angelina Titova:** Investigation. **Albina Malanyeva:** Investigation. **Olga Vasileva:** Investigation. **Kamil Gabdurakhmanov:** Investigation. **Sergei Dudnikov:** Investigation. **Lawrence M. Schopfer:** Writing – review & editing, Validation, Data curation. **Oksana Lockridge:** Writing – review & editing, Validation, Data curation. **Patrick Masson:** Writing – original draft, Supervision, Project administration, Funding acquisition, Conceptualization.

Declaration of competing interest

The authors declare no conflicts of interest.

Acknowledgement

This work was supported by the Russian Science Foundation grant N№ 20-14-00155 to PM and TP.

Appendix A. Supplementary materials

Supplementary data are available in the online version, at: https://doi.org/10.1016/j.ijbiomac.2024.137305

References

[1] M.R. Leung, L.S. van Bezouwen, L.M. Schopfer, J.L. Sussman, I. Silman, O. Lockridge, T. Zeev-Ben-Mordehai, Cryo-EM structure of the native butyrylcholinesterase tetramer reveals a dimer of dimers stabilized by a superhelical assembly, Proc. Natl. Acad. Sci. 115 (2018) 13270–13275, https://doi.org/10.1073/pnas.1817009115.

[2] K.M. Boyko, T.N. Baymukhametov, Y.M. Chesnokov, M. Hons, S.V. Lushchekina, P. V. Konarev, A.V. Lipkin, A.L. Vasiliev, P. Masson, V.O. Popov, M.V. Kovalchuk, 3D structure of the natural tetrameric form of human butyrylcholinesterase as revealed by cryoEM, SAXS and MD, Biochimie 156 (2019) 196–205, https://doi.org/10.1016/j.biochi.2018.10.017.

[3] Y. Nicolet, O. Lockridge, P. Masson, J.C. Fontecilla-Camps, F. Nachon, Crystal structure of human Butyrylcholinesterase and of its complexes with substrate and products, J. Biol. Chem. 278 (2003) 41141–41147, https://doi.org/10.1074/jbc.M210241200.

[4] I. Silman, The multiple biological roles of the cholinesterases, Prog. Biophys. Mol. Biol. 162 (2021) 41–56, https://doi.org/10.1016/j.pbiomolbio.2020.12.001.

[5] P. Masson, Z. Shaihutdinova, O. Lockridge, Drug and pro-drug substrates and pseudo-substrates of human butyrylcholinesterase, Biochem. Pharmacol. 218 (2023) 115910, https://doi.org/10.1016/j.bcp.2023.115910.

[6] T. Sun, T. Zhen, C.H. Harakandi, L. Wang, H. Guo, Y. Chen, H. Sun, New insights into butyrylcholinesterase: pharmaceutical applications, selective inhibitors and multitarget-directed ligands, Eur. J. Med. Chem. 275 (2024) 116569, https://doi.org/10.1016/j.ejmech.2024.116569.

[7] O. Lockridge, Review of human butyrylcholinesterase structure, function, genetic variants, history of use in the clinic, and potential therapeutic uses, Pharmacol. Ther. 148 (2015) 34–46, https://doi.org/10.1016/j.pharmthera.2014.11.011.

[8] D.M. Cerasoli, S.J. Armstrong, T.E. Reeves, S.M. Hodgins, S.A. Kasten, R.B. Lee-Stubbs, C.L. Cadieux, T.C. Otto, B.R. Capacio, D.E. Lenz, Butyrylcholinesterase, a stereospecific in vivo bioscavenger against nerve agent intoxication, Biochem. Pharmacol. 171 (2020) 113670, https://doi.org/10.1016/j.bcp.2019.113670.

[9] J.L. Allard, K.A. Shields, T.P. Munro, L.H.L. Lua, Strategies for developing a recombinant butyrylcholinesterase medical countermeasure for organophosphorus poisoning, Chem. Biol. Interact. 363 (2022) 109996, https://doi.org/10.1016/j.cbi.2022.109996.

[10] S. Lushchekina, P. Masson, Catalytic bioscavengers against organophosphorus agents: mechanistic issues of self-reactivating cholinesterases, Toxicology 409 (2018) 91–102, https://doi.org/10.1016/j.tox.2018.07.020.

[11] Z. Kovarik, M. Katalinić, G. Šinko, J. Binder, O. Holas, Y.-S. Jung, L. Musilova, D. Jun, K. Kuča, Pseudo-catalytic scavenging: searching for a suitable reactivator of phosphorylated butyrylcholinesterase, Chem. Biol. Interact. 187 (2010) 167–171, https://doi.org/10.1016/j.cbi.2010.02.023.

[12] Y.J. Rosenberg, R.J. Adams, S. Hernandez-Abanto, X. Jiang, W. Sun, L. Mao, K. D. Lee, Pharmacokinetics and immunogenicity of a recombinant human butyrylcholinesterase bioscavenger in macaques following intravenous and pulmonary delivery, Chem. Biol. Interact. 242 (2015) 219–226, https://doi.org/10.1016/j.cbi.2015.09.021.

[13] S. Terekhov, I. Smirnov, T. Bobik, O. Shamborant, M. Zenkova, E. Chernolovskaya, D. Gladkikh, A. Murashev, I. Dyachenko, V. Palikov, Y. Palikova, V. Knorre, A. Belogurov, N. Ponomarenko, G.M. Blackburn, P. Masson, A. Gabibov, A novel expression cassette delivers efficient production of exclusively tetrameric human butyrylcholinesterase with improved pharmacokinetics for protection against organophosphate poisoning, Biochimie 118 (2015) 51–59, https://doi.org/10.1016/j.biochi.2015.07.028.

[14] Y.-J. Huang, P.M. Lundy, A. Lazaris, Y. Huang, H. Baldassarre, B. Wang, C. Turcotte, M. Côté, A. Bellemare, A.S. Bilodeau, S. Brouillard, M. Touati, P. Herskovits, I. Bégin, N. Neveu, E. Brochu, J. Pierson, D.K. Hockley, D. M. Cerasoli, D.E. Lenz, H. Wilgus, C.N. Karatzas, S. Langermann, Substantially improved pharmacokinetics of recombinant human butyrylcholinesterase by fusion to human serum albumin, BMC Biotechnol. 8 (2008) 50, https://doi.org/10.1186/1472-6750-8-50.

[15] I. Schumacher, A. Arad, R. Margalit, Butyrylcholinesterase formulated in liposomes, Biotechnol. Appl. Biochem. 30 (1999) 225–230, https://doi.org/10.1111/j.1470-8744.1999.tb00774.x.

[16] S. Fischer, A. Arad, R. Margalit, Lipsome-formulated enzymes for organophosphate scavenging: Butyrylcholinesterase and Demeton-S, Arch. Biochem. Biophys. 434 (2005) 108–115, https://doi.org/10.1016/j.abb.2004.10.029.

[17] A. Gaydess, E. Duysen, Y. Li, V. Gilman, A. Kabanov, O. Lockridge, T. Bronich, Visualization of exogenous delivery of nanoformulated butyrylcholinesterase to the central nervous system, Chem. Biol. Interact. 187 (2010) 295–298, https://doi.org/10.1016/j.cbi.2010.01.005.

[18] K. Hester, J. Liu, N. Flynn, L.G. Sultatos, L. Geng, S. Brimijoin, J.D. Ramsey, S. Hartson, A. Ranjan, C. Pope, Polyionic complexes of butyrylcholinesterase and poly-l-lysine-g-poly(ethylene glycol): comparative kinetics of catalysis and inhibition and in vitro inactivation by proteases and heat, Chem. Biol. Interact. 275 (2017) 86–94, https://doi.org/10.1016/j.cbi.2017.07.019.

[19] P.N. Smith, L. Mao, K. Sinha, A.J. Russell, Organophosphate detoxification by membrane-engineered red blood cells, Acta Biomater. 124 (2021) 270–281, https://doi.org/10.1016/j.actbio.2021.01.043.

[20] V. Gupta, C.L. Cadieux, D. McMenamin, C.A. Medina-Jaszek, M. Arif, O. Ahonkhai, E. Wielechowski, M. Taheri, Y. Che, T. Goode, M.P. Limberis, M. Li, D.M. Cerasoli, A.P. Tretiakova, J.M. Wilson, Adeno-associated virus-mediated expression of human butyrylcholinesterase to treat organophosphate poisoning, PloS One 14 (2019) e0225188, https://doi.org/10.1371/journal.pone.0225188.

[21] P. Zhang, E.J. Liu, C. Tsao, S.A. Kasten, M.V. Boeri, T.L. Dao, S.J. DeBus, C. L. Cadieux, C.A. Baker, T.C. Otto, D.M. Cerasoli, Y. Chen, P. Jain, F. Sun, W. Li, H.-C. Hung, Z. Yuan, J. Ma, A.N. Bigley, F.M. Raushel, S. Jiang, Nanoscavenger provides long-term prophylactic protection against nerve agents in rodents, Sci. Transl. Med. 11 (2019) eaau7091, https://doi.org/10.1126/scitranslmed.aau7091.

[22] K. Kwon, J. Jung, A. Sahu, G. Tae, Nanoreactor for cascade reaction between SOD and CAT and its tissue regeneration effect, J. Control. Release 344 (2022) 160–172, https://doi.org/10.1016/j.jconrel.2022.02.033.

[23] J. Ming, T. Zhu, J. Li, Z. Ye, C. Shi, Z. Guo, J. Wang, X. Chen, N. Zheng, A novel Cascade Nanoreactor integrating two-dimensional Pd-Ru Nanozyme, Uricase and red blood cell membrane for highly efficient hyperuricemia treatment, Small 17 (2021) 2103645, https://doi.org/10.1002/smll.202103645.

[24] X. Geng, X. Du, W. Wang, C. Zhang, X. Liu, Y. Qu, M. Zhao, W. Li, M. Zhang, K. Tu, Y.-Q. Li, Confined Cascade metabolic reprogramming Nanoreactor for targeted alcohol detoxification and alcoholic liver injury management, ACS Nano 17 (2023) 7443–7455, https://doi.org/10.1021/acsnano.2c12075.

[25] T.N. Pashirova, A. Bogdanov, P. Masson, Therapeutic nanoreactors for detoxification of xenobiotics: concepts, challenges and biotechnological trends with special emphasis to organophosphate bioscavenging, Chem. Biol. Interact. 346 (2021) 109577, https://doi.org/10.1016/j.cbi.2021.109577.

[26] T. Pashirova, Z. Shaihutdinova, M. Mansurova, R. Kazakova, D. Shambazova, A. Bogdanov, D. Tatarinov, D. Daudé, P. Jacquet, E. Chabrière, P. Masson, Enzyme Nanoreactor for in vivo detoxification of organophosphates, ACS Appl. Mater. Interfaces (2022), https://doi.org/10.1021/acsami.2c03210.

[27] T. Pashirova, Z. Shaihutdinova, D. Tatarinov, M. Mansurova, R. Kazakova, A. Bogdanov, E. Chabrière, P. Jacquet, D. Daudé, A.A. Akhunzianov, R. R. Miftakhova, P. Masson, Tuning the envelope structure of enzyme Nanoreactors for in vivo detoxification of organophosphates, Int. J. Mol. Sci. 24 (2023) 15756, https://doi.org/10.3390/ijms242115756.

[28] P. Masson, S. Lushchekina, Conformational stability and denaturation processes of proteins investigated by electrophoresis under extreme conditions, Molecules 27 (2022) 6861, https://doi.org/10.3390/molecules27206861.

[30] Y. Wang, Q. Zhao, R. Haag, C. Wu, Biocatalytic synthesis using self-assembled polymeric Nano- and Microreactors, Angew. Chemie Int. Ed. 61 (2022), https://doi.org/10.1002/anie.202213974.

[31] D. Gaur, N.C. Dubey, B.P. Tripathi, Biocatalytic self-assembled synthetic vesicles and coacervates: from single compartment to artificial cells, Adv. Colloid Interface Sci. 299 (2022) 102566, https://doi.org/10.1016/j.cis.2021.102566.

[32] G. Sinsinbar, A.K. Bindra, S. Liu, T.W. Chia, E.C. Yoong Eng, S.Y. Loo, J.H. Lam, K. Schultheis, M. Nallani, Amphiphilic block copolymer nanostructures as a tunable delivery platform: perspective and framework for the future drug product development, Biomacromolecules 25 (2024) 541–563, https://doi.org/10.1021/acs.biomac.3c00858.

[33] M.G. Gouveia, J.P. Wesseler, J. Ramaekers, C. Weder, P.B.V. Scholten, N. Bruns, Polymersome-based protein drug delivery – quo vadis? Chem. Soc. Rev. 52 (2023) 728–778, https://doi.org/10.1039/D2CS00106C.

[34] S.D. Allen, Y.-G. Liu, S. Bobbala, L. Cai, P.I. Hecker, R. Temel, E.A. Scott, Polymersomes scalably fabricated via flash nanoprecipitation are non-toxic in non-human primates and associate with leukocytes in the spleen and kidney following intravenous administration, Nano Res. 11 (2018) 5689–5703, https://doi.org/10.1007/s12274-018-2069-x.

[35] E.G. Duysen, O. Lockridge, Whole body and tissue imaging of the butyrylcholinesterase knockout mouse injected with near infrared dye labeled butyrylcholinesterase, Chem. Biol. Interact. 175 (2008) 119–124, https://doi.org/10.1016/j.cbi.2008.02.011.
[36] N.D. Johnson, E.G. Duysen, O. Lockridge, Intrathecal delivery of fluorescent labeled butyrylcholinesterase to the brains of butyrylcholinesterase knock-out mice: visualization and quantification of enzyme distribution in the brain, Neurotoxicology 30 (2009) 386–392, https://doi.org/10.1016/j.neuro.2009.03.001.
[37] H. Li, X.-D. Li, C.-H. Yan, Z.-H. Ni, M.-H. Lü, L.-W. Zou, L. Yang, Rational design of a near-infrared fluorescent probe for monitoring butyrylcholinesterase activity and its application in development of inhibitors, Front. Bioeng. Biotechnol. 12 (2024), https://doi.org/10.3389/fbioe.2024.1387146.
[38] B. Yang, Y. He, X. Ding, Z. Liu, X. Wang, W. Yu, Exploring butyrylcholinesterase expression in living cells and diabetic mouse models using a fluorescent probe with near-infrared excitation and emission maxima, Dyes Pigments 229 (2024) 112295, https://doi.org/10.1016/j.dyepig.2024.112295.
[39] L.M. Schopfer, E. David, S.H. Hinrichs, O. Lockridge, Human butyrylcholinesterase in Cohn fraction IV-4 purified in a single chromatography step on Hupresin, PloS One 18 (2023) e0280380, https://doi.org/10.1371/journal.pone.0280380.
[40] G.L. Ellman, K.D. Courtney, V. Andres, R.M. Featherstone, A new and rapid colorimetric determination of acetylcholinesterase activity, Biochem. Pharmacol. 7 (1961) 88–95, https://doi.org/10.1016/0006-2952(61)90145-9.
[41] W. Leuzinger, The number of catalytic sites in acetylcholinesterase, Biochem. J. 123 (1971) 139–141, https://doi.org/10.1042/bj1230139.
[42] S. Cerritelli, D. Velluto, J.A. Hubbell, PEG-SS-PPS: reduction-sensitive disulfide block copolymer vesicles for intracellular drug delivery, Biomacromolecules 8 (2007) 1966–1972, https://doi.org/10.1021/bm070085x.
[43] D. Velluto, D. Demurtas, J.A. Hubbell, PEG- b -PPS Diblock copolymer aggregates for hydrophobic drug Solubilization and release: Cyclosporin a as an example, Mol. Pharm. 5 (2008) 632–642, https://doi.org/10.1021/mp7001297.
[44] M. Satou, T. Fujihara, J. Terao, Y. Tsuji, Synthesis and characterization of carboxylic acids bearing poly(ethylene glycol) chains, Synlett 29 (2018) 556–559, https://doi.org/10.1055/s-0036-1591840.
[45] A. Napoli, N. Tirelli, G. Kilcher, A. Hubbell, New synthetic methodologies for amphiphilic multiblock copolymers of ethylene glycol and propylene sulfide, Macromolecules 34 (2001) 8913–8917, https://doi.org/10.1021/ma0108057.
[46] M.-L. Laracuente, M.H. Yu, K.J. McHugh, Zero-order drug delivery: state of the art and future prospects, J. Control. Release 327 (2020) 834–856, https://doi.org/10.1016/j.jconrel.2020.09.020.
[47] S. Bhattacharjee, Understanding the burst release phenomenon: toward designing effective Nanoparticulate drug-delivery systems, Ther. Deliv. 12 (2021) 21–36, https://doi.org/10.4155/tde-2020-0099.
[48] X. Huang, C.S. Brazel, On the importance and mechanisms of burst release in matrix-controlled drug delivery systems, J. Control. Release 73 (2001) 121–136, https://doi.org/10.1016/S0168-3659(01)00248-6.
[49] J. Yoo, Y.-Y. Won, Phenomenology of the initial burst release of Drugs from PLGA microparticles, ACS Biomater Sci. Eng. 6 (2020) 6053–6062, https://doi.org/10.1021/acsbiomaterials.0c01228.
[50] C. Hua, L. Qiu, Polymersomes for therapeutic protein and peptide delivery: towards better loading properties, Int. J. Nanomedicine 19 (2024) 2317–2340, https://doi.org/10.2147/IJN.S444910.
[51] B.P. Doctor, A. Saxena, Bioscavengers for the protection of humans against organophosphate toxicity, Chem. Biol. Interact. 157–158 (2005) 167–171, https://doi.org/10.1016/j.cbi.2005.10.024.
[52] E.G. Duysen, C.F. Bartels, O. Lockridge, Wild-type and A328W mutant human Butyrylcholinesterase tetramers expressed in Chinese Hamster ovary cells have a 16-hour half-life in the circulation and protect mice from cocaine toxicity, J. Pharmacol. Exp. Ther. 302 (2002) 751–758, https://doi.org/10.1124/jpet.102.033746.
[53] P. Wen, W. Ke, A. Dirisala, K. Toh, M. Tanaka, J. Li, Stealth and pseudo-stealth nanocarriers, Adv. Drug Deliv. Rev. 198 (2023) 114895, https://doi.org/10.1016/j.addr.2023.114895.
[54] P.J. Photos, L. Bacakova, B. Discher, F.S. Bates, D.E. Discher, Polymer vesicles in vivo: correlations with PEG molecular weight, J. Control. Release 90 (2003) 323–334, https://doi.org/10.1016/S0168-3659(03)00201-3.
[55] J.S. Lee, M. Ankone, E. Pieters, R.M. Schiffelers, W.E. Hennink, J. Feijen, Circulation kinetics and biodistribution of dual-labeled polymersomes with modulated surface charge in tumor-bearing mice: comparison with stealth liposomes, J. Control. Release 155 (2011) 282–288, https://doi.org/10.1016/j.jconrel.2011.07.028.
[56] A.L. Klibanov, K. Maruyama, V.P. Torchilin, L. Huang, Amphipathic polyethyleneglycols effectively prolong the circulation time of liposomes, FEBS Lett. 268 (1990) 235–237, https://doi.org/10.1016/0014-5793(90)81016-H.
[57] J.L. Perry, K.G. Reuter, M.P. Kai, K.P. Herlihy, S.W. Jones, J.C. Luft, M. Napier, J. E. Bear, J.M. DeSimone, PEGylated PRINT nanoparticles: the impact of PEG density on protein binding, macrophage association, biodistribution, and pharmacokinetics, Nano Lett. 12 (2012) 5304–5310, https://doi.org/10.1021/nl302638g.
[58] A. Najer, O. Rifaie-Graham, J. Yeow, C. Adrianus, M. Chami, M.M. Stevens, Differences in human plasma protein interactions between various Polymersomes and stealth liposomes as observed by fluorescence correlation spectroscopy, Macromol. Biosci. (2022) 2200424, https://doi.org/10.1002/mabi.202200424.
[59] M. Kumar, P. Kulkarni, S. Liu, N. Chemuturi, D.K. Shah, Nanoparticle biodistribution coefficients: a quantitative approach for understanding the tissue distribution of nanoparticles, Adv. Drug Deliv. Rev. 194 (2023) 114708, https://doi.org/10.1016/j.addr.2023.114708.
[60] E. Sadauskas, H. Wallin, M. Stoltenberg, U. Vogel, P. Doering, A. Larsen, G. Danscher, Kupffer cells are central in the removal of nanoparticles from the organism, Part. Fibre Toxicol. 4 (2007) 10, https://doi.org/10.1186/1743-8977-4-10.
[61] W. Poon, Y.-N. Zhang, B. Ouyang, B.R. Kingston, J.L.Y. Wu, S. Wilhelm, W.C. W. Chan, Elimination pathways of nanoparticles, ACS Nano 13 (2019) 5785–5798, https://doi.org/10.1021/acsnano.9b01383.
[62] W. Ngo, S. Ahmed, C. Blackadar, B. Bussin, Q. Ji, S.M. Mladjenovic, Z. Sepahi, W.C. W. Chan, Why nanoparticles prefer liver macrophage cell uptake in vivo, Adv. Drug Deliv. Rev. 185 (2022) 114238, https://doi.org/10.1016/j.addr.2022.114238.
[63] D. Ezhilarasan, K. Shree Harini, Nanodrug delivery: strategies to circumvent nanoparticle trafficking by Kupffer cells in the liver, J. Drug Deliv. Sci. Technol. 86 (2023) 104731. doi:https://doi.org/10.1016/j.jddst.2023.104731.
[64] Z. Shajhutdinova, T. Pashirova, P. Masson, Kinetic processes in enzymatic Nanoreactors for in vivo detoxification, Biomedicines 10 (2022) 784, https://doi.org/10.3390/biomedicines10040784.
[65] L. Pei, G. Omburo, W.D. Mcguinn, I. Petrikovics, K. Dave, F.M. Raushel, J.R. Wild, J.R. Deloach, J.L. Way, Encapsulation of Phosphotriesterase within murine erythrocytes, Toxicol. Appl. Pharmacol. 124 (1994) 296–301, https://doi.org/10.1006/taap.1994.1035.
[66] L. Koleva, E. Bovt, F. Ataullakhanov, E. Sinauridze, Erythrocytes as carriers: from drug delivery to biosensors, Pharmaceutics 12 (2020) 276, https://doi.org/10.3390/pharmaceutics12030276.
[67] E. Udofa, Z. Zhao, In situ cellular hitchhiking of nanoparticles for drug delivery, Adv. Drug Deliv. Rev. 204 (2024) 115143, https://doi.org/10.1016/j.addr.2023.115143.